Journal of Nuclear Materials 377 (2008) 486–491

Contents lists available at ScienceDirect

Journal of Nuclear Materials

journal homepage: www.elsevier.com/locate/jnucmat

# Structural investigation of re-deposited layers in JET

J. Likonen [a,*], E. Vainonen-Ahlgren [a], L. Khriachtchev [b], J.P. Coad [c], M. Rubel [d], T. Renvall [a], K. Arstila [e], D.E. Hole [f], Contributors to the EFDA-JET Work-programme

[a] VTT, Materials and Building, Association EURATOM-TEKES, P.O. Box 1000, 02044 VTT, Finland
[b] Laboratory of Physical Chemistry, University of Helsinki, Association EURATOM-TEKES, P.O. Box 55, 00014 Helsinki, Finland
[c] UKAEA Fusion, UKAEA/EURATOM Fusion Association, Abingdon, Oxon, OX14 4DB, UK
[d] Alfvén Laboratory, Royal Institute of Technology, Association EURATOM-VR, 100 44 Stockholm, Sweden
[e] Accelerator Laboratory, University of Helsinki, Association EURATOM-TEKES, P.O. Box 43, 00014 Helsinki, Finland
[f] School of Engineering, University of Sussex, Brighton, BN1 9QH, East Sussex, UK

ARTICLE INFO

*Article history:*
Received 1 February 2008
Accepted 14 April 2008

ABSTRACT

JET Mk-II Gas Box divertor tiles exposed in 1998–2001 have been analysed with various ion beam techniques, secondary ion mass spectrometry (SIMS) and Raman spectroscopy. Inner divertor wall tiles removed in 2001 were covered with a duplex film. The inner layer was very rich in metallic impurities, with Be/C ~ 1 and H-isotopes only present at low concentrations. The outer layer contained higher concentrations of D than normal for plasma-facing surfaces in JET (D/C ~ 0.4), and Be/C ~ 0.14. Raman and SIMS analyses show that the deposited films on inner divertor tiles are hydrogenated amorphous carbon with low $sp^3$ fractions. The deposits have polymeric structure and low density. Both Raman scattering and SIMS indicate that films on inner divertor wall Tiles 1 and 3, and on floor Tile 4 have some differences in the chemical structure of the deposited films

© 2008 Elsevier B.V. All rights reserved.

## 1. Introduction

Thin film formation of plasma-facing components (PFCs) is an important subject in fusion reactor development because the re-deposited layers will affect the lifetime of the PFC, the tritium inventory and tritium recycling. Carbon based materials have been used as low-Z plasma-facing materials in fusion devices for a long time because of their good thermo-physical properties. Unfortunately, carbon is chemically eroded by hydrogen ions due to chemical sputtering. Erosion of carbon in the plasma edge generates mobile particles which migrate to other parts of the fusion reactor and deposit to form a film. The deposited carbon film not only affect the sputtering of the plasma-facing material but also acts as a depository for hydrogen isotopes.

Deposition in JET divertor tiles has been observed to be asymmetric; i.e. heavy deposition occurs in the scrape-off layer (SOL) at the inner divertor whereas there is little deposition at the outer divertor [1,2]. Heavy deposition at the inner divertor has led to flaking on the water-cooled louvres and after the DTE1 tritium experiment at JET it was observed that the majority of the retained tritium is in flakes that have spalled from the louvres. The asymmetry in the deposition implies a drift in the SOL from outboard to inboard, as has been seen in JET using reciprocating probes [3]. The deposition at the inner divertor, as analysed when tiles were removed from the vessel, is the result of typically 2 years of JET operations with about 4500 discharges covering many types of operation. It is thus difficult to tell which aspects of operation are important in controlling the deposition, and effects summarized over numerous parameters and factors can be studied. In this study, the composition of the re-deposited layers have been analysed using SIMS, Rutherford backscattering spectroscopy (RBS), nuclear reaction analysis (NRA) and time-of-flight elastic recoil detection analysis (TOF-ERDA). Raman spectroscopy has been utilised for structural analysis.

## 2. Experimental

JET is operated with PFC made of carbon (CFC, Concept I manufactured by Dunlop Ltd.). The main chamber wall is coated periodically with a thin beryllium layer produced by evaporation using either two or four Be evaporator heads located in the equatorial plane of the torus. The Gas Box divertor (Mk-IIGB) was first installed in 1998 during the remote tile exchange (RTE) shutdown. A set of divertor tiles analysed in this work was exposed throughout the lifetime of the Mk-IIGB divertor, i.e. during 1998–2001. During the last day of the C4 campaign in 2001, pure $^{13}CH_4$ was injected through gas introduction module (GIM) at the top of the vessel (GIM 5) for up to 10 s in 13 pulses. GIM5 injects at one toroidal location only, in octant 5. The total number of $^{13}C$ atoms introduced was $1.3 \times 10^{23}$ [4].

* Corresponding author. Tel.: +358 20 7226364; fax: +358 20 7226390.
*E-mail address:* jari.likonen@vtt.fi (J. Likonen).

0022-3115/$ - see front matter © 2008 Elsevier B.V. All rights reserved.
doi:10.1016/j.jnucmat.2008.04.005

During the Mk-IIIGB campaign in 1998–2001 the strike points were most frequently on the vertical Tiles 3 and 7 at various locations (see Fig. 1). Very occasionally the strike point was moved onto the vertical Tiles 1 and 8. Moreover, there was a limited range of plasma configurations with the strike points on Tiles 4 and/or 6. Most of the surfaces of Tiles 4 and 6 are horizontal (see Fig. 1), but the possible strike point positions were restricted to the sloping parts of the tiles between horizontal parts shadowed by the septum structure and by Tiles 3 or 7. The plasma configurations with the strike points on the floor tiles ('corner shots') were quite frequently run in studies of divertor physics allowing access to the cryopump from the scrape-off layer (SOL) rather than from the private flux region. The corner shots were also believed to be very important for material transport and retention.

JET has normally operated with a vessel wall temperature of 320 °C. However, since beginning of 2001 the vessel temperature was held at 200 °C throughout the two-month operations in 2001 prior to the shutdown. The JET divertor is water-cooled and thus the divertor tiles have a base temperature intermediate between the water and vessel temperatures. Thermocouples are embedded in some of the tiles that continually monitor the bulk tile temperature. During the MK- IIGB operations in 2001 Tiles 1, 3 and 4 had base temperatures of 110, 120 and 100 °C, respectively. During each plasma discharge (in the divertor configuration) power is deposited on the tile surfaces: the strike point region may reach 1000 °C or greater and the overall energy deposited in the divertor may be 10 MJ. Thus, during a day of plasma pulsing the bulk temperature of the tiles steadily increases, typically to 140 °C for Tiles 1 and 3, respectively, returning to the base temperature overnight. The maximum temperatures of Tiles 1, 3 and 4 averaged over the campaign are 130, 140 and 130 °C, respectively.

After removal of the divertor tiles from the torus a set of samples of 17 mm in diameter was cut using a coring technique [4]. The poloidal positions of the samples are shown in Fig. 1.

The Raman measurements were performed in the 100–3000 $cm^{-1}$ region by using a single-stage spectrometer (Acton SpectraPro 500I) in a low-resolution mode (resolution ~ 10 $cm^{-1}$) equipped with a 1024 × 256 pixel CCD camera (Andor InstaSpec IV). Radiation of an $Ar^+$ laser (Omnichrome 543-AP, 514.5 nm, ~50 mW) was directed to a film at ~45° in P-polarization and focused to a ~50-μm spot. The Raman scattering light was transmitted without polarization analysis through a collecting optics, a holographic filter (Kaiser Super-Notch-Plus), and an optical fiber. In order to analyze amorphous carbon, the Raman spectra are fitted with two conventional bands (so-called D and G peaks) [5,6]. The experimental details and methodologies are described elsewhere [7]. The fitting is complicated by the presence of strong photoluminescence (PL) from the present samples. Several fitting procedures have been tested: (i) two Lorentzians for D and G peaks and a linear background for PL, (ii) two Gaussians for D and G peaks and a linear background for PL (additionally, one or two Gaussians could be used to improve fitting the band wings), and (iii) two Gaussians for D and G peaks and the third Gaussian for PL. The results with the last procedure seem to be the most satisfactory.

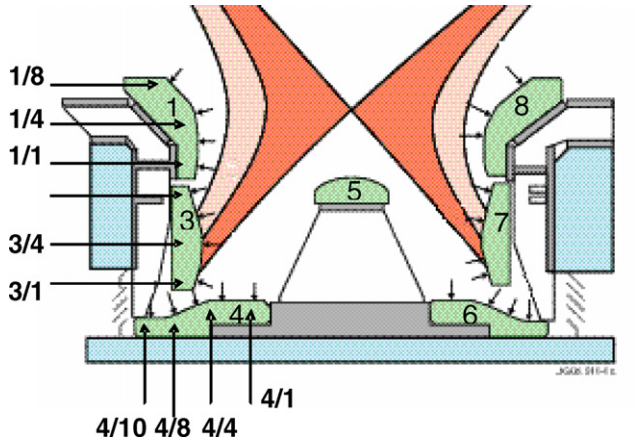


**Fig. 1.** The JET Mk-IIGB divertor tile set. The samples for SIMS and IBA measurements are indicated with numbers. The first number in the sample code refers to divertor tile and the second one to the position in the tile.

The SIMS analysis was made with a double focussing magnetic sector instrument (VG Ionex IX-70S). A 5 keV $O_2^+$ primary ion beam was used. The current of the primary ion beam was typically 500 nA during depth profiling and the ion beam was raster-scanned over an area of 300 × 430 $\mu m^2$. Since the surface topography of the CFC tiles varies, SIMS measurements are performed at several points on each sample, covering an area larger than the fibre plane separation. The mass spectra were measured using 22 keV $Ga^+$ primary ions with a current of 20 nA. In this case the ion beam was raster-scanned over an area of 240 × 350 $\mu m^2$.

The TOF-ERDA measurements of elementary concentration profiles were performed with the 5-MV tandem accelerator EGP-10-II of the University of Helsinki. In the measurements, a 53-MeV beam of $^{127}I^{10+}$ ions was used. The detector angle was 40°, and the samples were tilted relative to the beam direction by 20°. The elementary concentrations were calculated using known geometry and SRIM-96 stopping powers in energy-loss calculations [8]. The maximum analysis depth was about 1 μm. The experimental set-up of RBS and NRA measurements is presented elsewhere [9].

## 3. Results and discussion

The normal pattern of material migration seen at JET is deposition at the inner divertor target and some erosion at the outer. The deposited material is mainly carbon with hydrogen isotopes, beryllium and oxygen. The samples analysed in this work are mainly from the inner divertor. The model for carbon transport in the Mk-IIGB divertor for the period 1998–2001 remains transport of impurities along the SOL to the inner divertor, followed by chemical sputtering of carbon from the inner divertor wall. The carbon will proceed in erosion/ionisation/re-deposition steps until it reaches the sloping part of the inner floor Tile 4.

The SIMS measurements have been made on a number of samples from each divertor tile. Typical SIMS depth profiles from three tile samples are shown in Fig. 2. Sample 1/1 is from the bottom of the front face of Tile 1 (Fig. 2(a)), sample 3/4 is from the centre of Tile 3 (Fig. 2(b)), and sample 4/10 is from the part of Tile 4 shadowed from the plasma by Tile 3 (Fig. 2(c)). The SIMS depth profiles of sample 1/1 and 3/4 shows a double layer structure which was observed also in tiles exposed in 1999–2001 [9]. The surface layers (approx. 5–8 μm and 10–30 μm thick on Tile 1 and 3, respectively) contain mostly C and D together with B and Ni of the Inconel steel which is used in the JET vessel wall and for internal metal fittings, bolts etc. RBS and TOF-ERDA analyses show that B and Ni contents are low (<1 at.%). The films underneath the surface layer are very rich in beryllium, and nickel peaks in this region. Layers rich in metals, and depleted in carbon, have been found at the inner divertor wall previously [1,2].

The surface compositions of samples 1/1 and 3/4 are quite different to those deeper into the deposit, being mostly C and Be (with some Ni), and with a higher deuterium content. The composition of this part of the film is similar to that found in deposits at the sides of limiters in the main chamber, and presumably to that arriving at the inner divertor along the SOL. It thus appears that during the last part of the campaign, carbon was no longer being chemically sputtered from the films. The origin of this outer layer

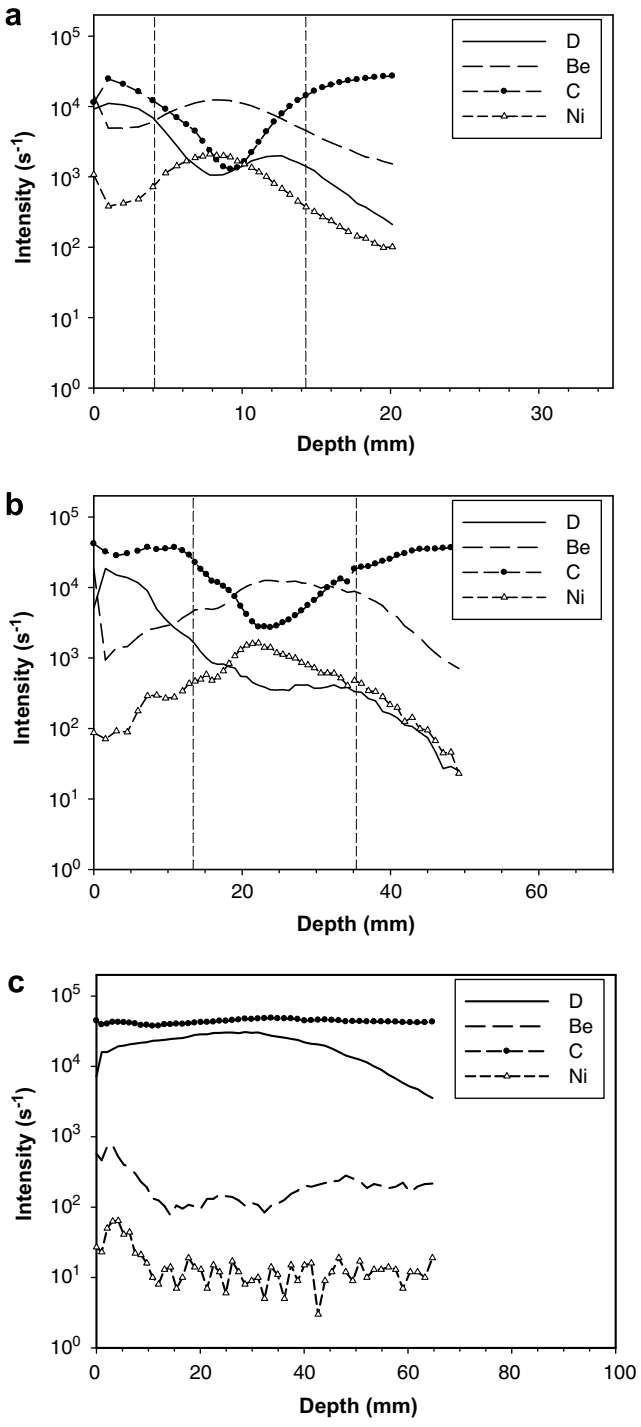


**Fig. 2.** SIMS depth profiles of D, Be, C and Re from (a) sample 1/1, (b) sample 3/4 and (c) from sample 4/10. Samples were exposed in 1998–2001. Vertical dashed lines show the approximate positions of the interfaces.

results from the four weeks of operation in helium prior to the 2001 opening [10].

The layered structure observed in SIMS depth profiles (including the surface deposition of $^{13}C$) have been simulated with the SIMNRA program [11] for many RBS spectra from Tile 1. Fig. 3 shows the experimental and the simulated RBS spectrum for a point towards the bottom of the tile. The deposited film was modelled by using three different layers in the simulations, since there are clearly at least three identifiable layers from SIMS data; a thin outer layer containing the $^{13}C$, and the two parts of the main film.

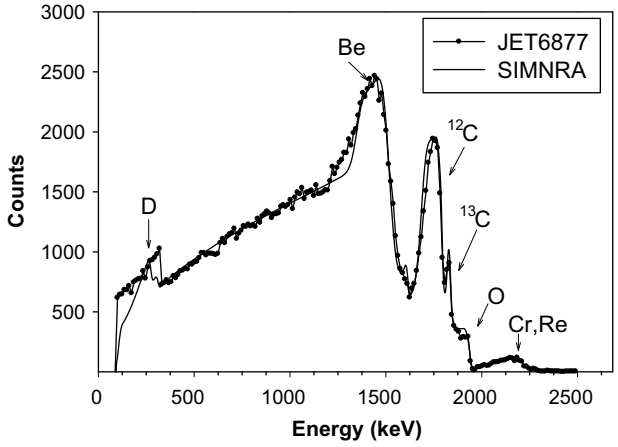


**Fig. 3.** Experimental (JET6877) and SIMNRA simulated Rutherford backscattering spectra from the bottom of Tile 1 exposed in 1998–2001.

The results of the simulation at this stage, which gives the fit shown in Fig. 3, are collected in Table 1. Qualitatively the RBS spectrum is totally consistent with the SIMS three-layer picture of a thin $^{13}C$ layer on top of one layer rich in $^{12}C$ and D and a second layer on the surface of the CFC substrate containing carbon and a large fraction of beryllium oxide.

Mk-IIGB tiles showed thick films of high D/C ratio with no Be and other metallic impurities on the part of Tile 4 shadowed by Tile 3. Somewhat thinner films (~15 μm) are also seen in the region of the Mk-IIGB Tile 4 shadowed by the septum. In this region the films have a D/C concentration ratio of ~0.4 and also negligible Be and other metallic impurities. In the more central region of Tile 4, including the sloping section of the tile, D contents are much lower and sometimes concentrated at the surface, and traces of Be are visible.

Structural analysis of the deposits on inner divertor tiles was investigated with SIMS and Raman spectroscopy. Fig. 4(a)–(c) shows negative ion mass spectra for graphite, DLC coating with high amount of $sp^3$ bonds and sample 3/4, respectively. In addition to hydrocarbon peaks there are impurity peaks such as F and Cl. The $C_x^-$ cluster peaks are also observed in the spectra. In the negative ion spectra of graphite (Fig. 4(a)) and DLC (Fig. 4(b)) dominating peaks are $C_x^-$ clusters. $GaO_2$ peaks in the DLC spectrum are due to recombination of $Ga^+$ primary ions with $O_2$ molecules after sputtering. The spectrum for sample 3/4 (Fig. 4(c)) exhibits the C, O and hydrocarbon peaks. $C_x^-$ cluster peaks are observed up to $x = 3$ only. The peaks with $x > 3$ are observed in the spectra for graphite and DLC coating only.

Fig. 5 shows the measured signal intensity of $C_x^-$ clusters as a function of cluster size for sample 3/4. Clusters with size up to 10 atoms were recorded in the negative ion mass spectra. The signal intensities of the $C_x^-$ clusters decrease exponentially as a function of the cluster size. A linear fit can be made to the data points and regression line can be drawn through the logarithm of the $C_x^-$ intensities. The absolute value of its slope is called a fragmentation factor ($F$) which measures the contribution of the small fragments

**Table 1**
Results of SIMNRA simulations of an RBS spectrum (JET6877) recorded from near the bottom of Tile 1

| Layer | D (at.%) | Be (at.%) | $^{12}C$ (at.%) | $^{13}C$ (at.%) | O |
|---|---|---|---|---|---|
| 1 | 10 | 8 | 45 | 26 | 11 |
| 2 | 27 | 5 | 53 | 0 | 15 |
| 3 | 11 | 36 | 24 | 0 | 29 |

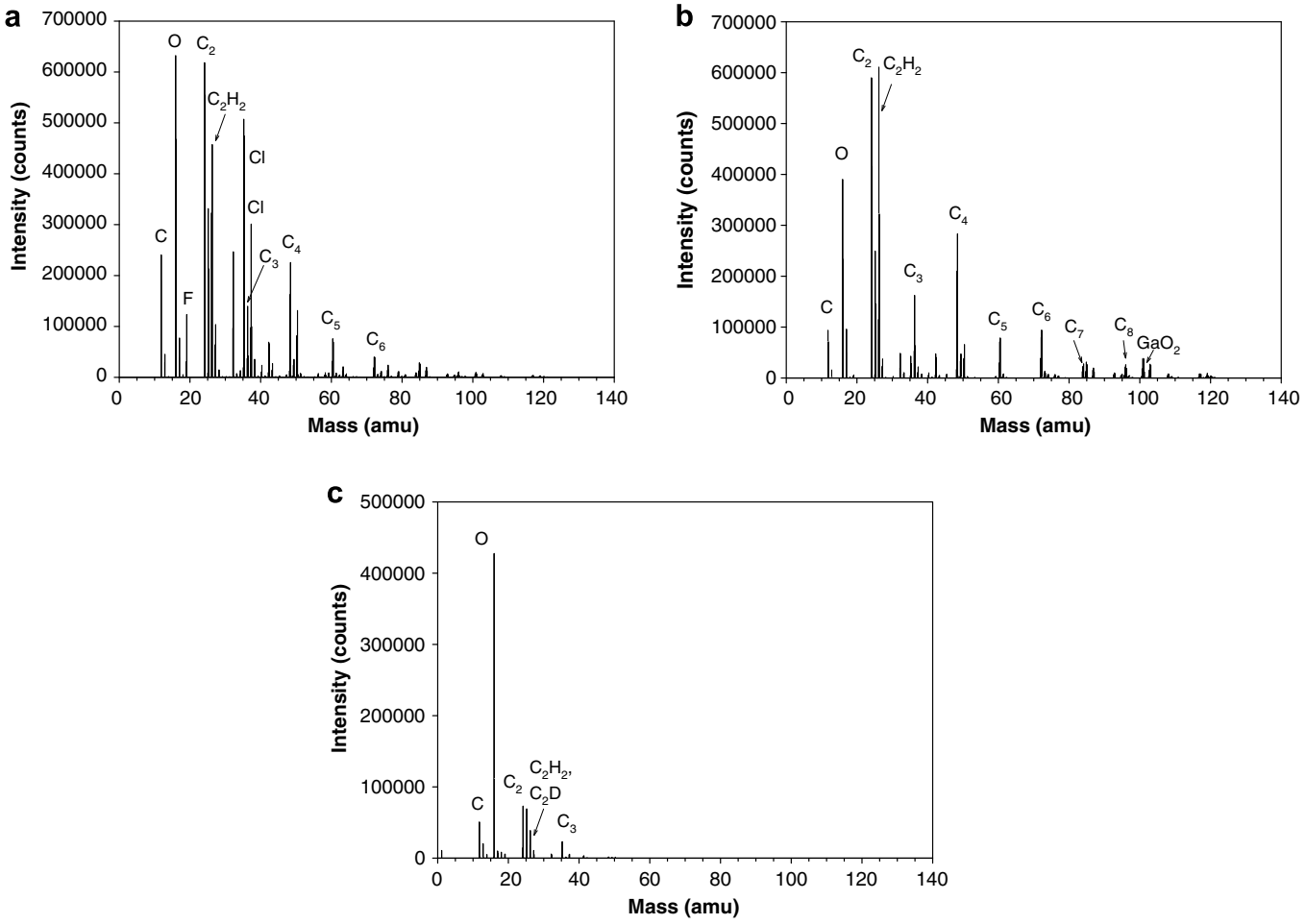


**Fig. 4.** SIMS negative ion mass spectrum for (a) graphite, (b) DLC coating, and (c) sample 3/4 (from the centre of Mk-IIGB tile 3).

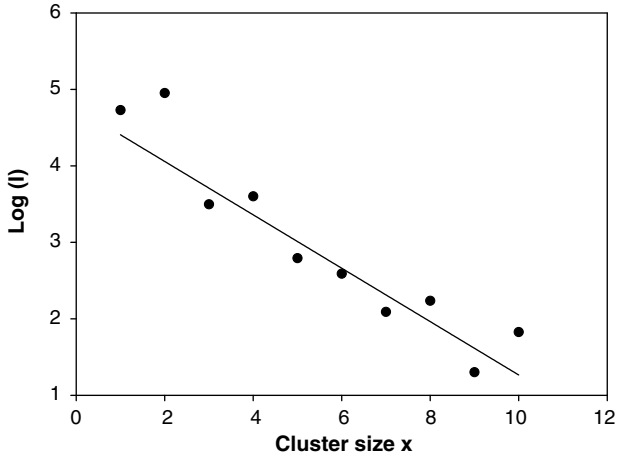


**Fig. 5.** Logarithm of signal intensity of $C_x^-$ clusters as a function of cluster size for sample 3/4 (from the centre of Mk-IIGB tile 3). Linear curve is least-square fit to the data points.

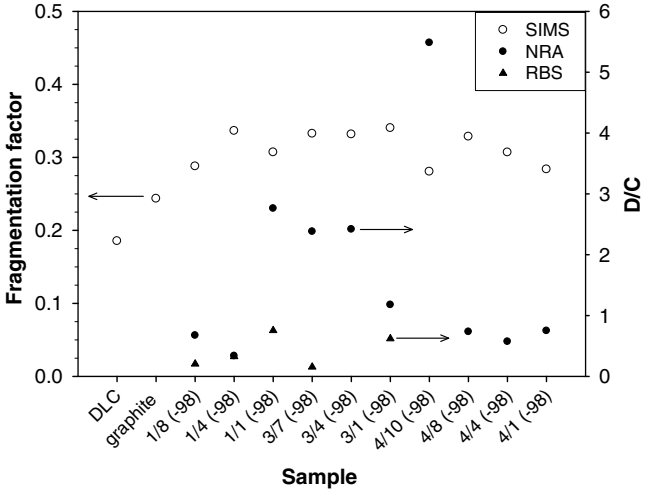


**Fig. 6.** Fragmentation factor for analysed samples. D/C ratio was measured using NRA and RBS techniques.

to the total emission [12]. The existing models for secondary ion emission suggest that the constituent atoms of large clusters should originate from adjacent sites on the surface [13–15]. The fragmentation factor is empirically related to the coordination of the carbon at the surface of the source of the ions. The smaller value of *F* correlates with the higher coordination (i.e. $sp^3$ versus $sp^2$ and $sp^1$ content).

The fragmentation factors for the analysed samples are shown in Fig. 6. It can be seen that DLC coating has the smallest fragmentation factor, as can be expected from high coordination number (i.e. high amount of $sp^3$ bonds). Graphite has a bigger fragmentation factor which can be attributed to the $sp^2$ bonds. All the analysed JET samples have larger fragmentation factors than

graphite indicating lower coordination number (i.e. a mixture of $sp^1$ and $sp^2$ bonded atoms). In practise the hybridisation is mixed, such as $sp^1$–$sp^2$. As can be seen from the figure, the fragmentation factor for the samples from Tile 3 is higher than those for the samples from Tile 4, indicating lower hybridisation of films on Tile 3. D/C ratio from RBS and NRA analyses is also presented in Fig. 6. There does not seem to be any clear correlation between the D/C concentration ratio and the fragmentation factor. The discrepancy between RBS and NRA results for samples from Tiles 1 and 3 is due to that the deposited films are too thick to be detected completely with RBS.

A typical example of the measured Raman spectra with decomposition into the D and G peaks is presented in Fig. 7. The extracted parameters are given in Table 2. The deposited material is amorphous as evidenced by the relatively broad D and G peaks (~200 and 100 $cm^{-1}$, respectively), as compared, for example, with pyrolytic graphite (~60 and 40 $cm^{-1}$, respectively). The positions of the D and G peaks at $cm^{-1}$ are typical for hydrogenated amorphous carbon with low $sp^3$ fractions. The relatively narrow G lines (FWHM ~ 100 $cm^{-1}$) are a typical fingerprint of the presence of

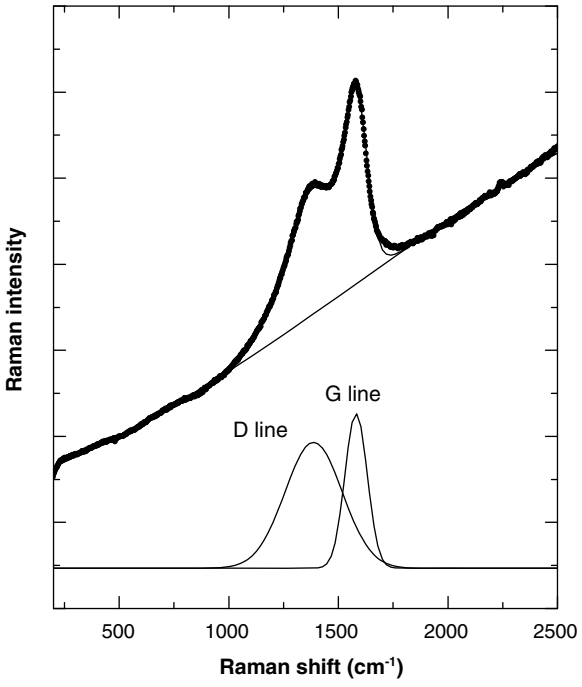


**Fig. 7.** Raman spectrum of sample 1/1. The Gaussian decomposition into D and G peaks and subtraction of the PL is shown.

**Table 2**
Raman parameters of the amorphous carbon samples exposed in 1998–2001

| Sample | H + D (%) | D-line position ($cm^{-1}$) | D-line width ($cm^{-1}$) | G-line position ($cm^{-1}$) | G-line width ($cm^{-1}$) | D/G intensity ratio |
|---|---|---|---|---|---|---|
| 1/1 | 18 | 1387 | 242 | 1580 | 98 | 1.8 |
| | | 1387 | 226 | 1576 | 98 | 1.6 |
| ¾ | 22.7 | 1387 | 230 | 1573 | 98 | 1.7 |
| | | 1385 | 223 | 1574 | 99 | 1.6 |
| 3/1 | 22.5 | 1382 | 205 | 1584 | 91 | 1.6 |
| | | 1382 | 207 | 1583 | 92 | 1.6 |
| 4/1 | 9.7 | 1367 | 233 | 1561 | 110 | 1.7 |
| | | 1362 | 216 | 1558 | 112 | 1.4 |
| 4/10 | 31.8 | 1374 | 220 | 1574 | 107 | 1.5 |
| | | 1380 | 218 | 1572 | 111 | 1.3 |

Two points were measured for each sample.

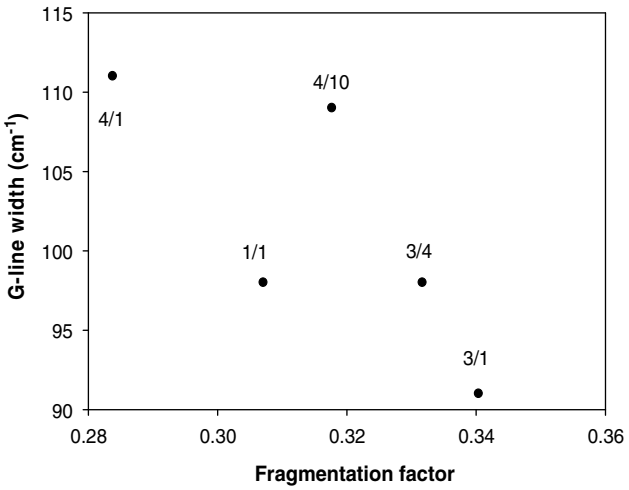


**Fig. 8.** G-line width as a function of fragmentation factor.

hydrogen in the network whereas hydrogen-free carbon materials usually exhibit G line widths of $\geqslant$200 $cm^{-1}$ [6,16]. The G peak width of ~100 $cm^{-1}$ also indicates soft material (hardness < 10 GPa) and low density (<1.6 g/$cm^3$). The more narrow G lines obtained for sample 3/1 suggest that this material has a lower coordination number than in sample 4/1, which is in agreement with the results obtained from the fragmentation factors (see Fig. 6). The optical gap is probably 1.0–1.2 eV as indicated by the G line position above 1560 $cm^{-1}$ and the D/G intensity ratio of 0.9–1.5 [6] (see Fig. 8).

Strong photoluminescence was found for most of the analysed samples, and this is characteristic for hydrogenated carbon with rather polymeric structure that has a significant portion of $sp^1$ carbon atoms [5,17]. These characteristics are typical for hydrogenated amorphous carbon with low $sp^3$ fractions. The photoluminescence is stronger for sample 3/1 than for sample 4/1, which agrees with the results obtained with fragmentation factors.

Based on the Raman data all the measured samples are structurally relatively similar, and the small differences (see Table 2) can be caused by variation of the hydrogen concentration or/and of the deposition conditions (for instance, the deposition angle [18]). The existing knowledge in the area does not allow analysing more conclusively these small differences when the hydrogen concentration changes from sample to sample and the depositions condition are uncontrolled because the plasma parameters vary at the divertor. In addition, the strong photoluminescence decreases accuracy of the extracted Raman parameters. The metallic impurities further complicate the analysis [18]. Supporting this limitation for analysis, our attempts to find systematic correlation between the Raman parameters, which are known in literature for hydrogenated carbon [6], partially failed due to relatively small variations of the parameters.

## 4. Conclusions

JET divertor tiles exposed in 1998–2001 have been analysed with various ion beam techniques, SIMS and Raman spectroscopy. Inner divertor wall tiles removed in 2001 were covered with a duplex film. The inner layer was very rich in metallic impurities, with Be/C ~ 1 and H-isotopes only present at low concentrations. The outer layer contained higher concentrations of D than normal for plasma-facing surfaces in JET (D/C ~ 0.4), and Be/C ~ 0.14.

Raman and SIMS analyses show that the deposited films on inner divertor tiles are hydrogenated amorphous carbon with low $sp^3$ fractions. The deposits have polymeric structure with a $sp^1$

fraction and low density. Both Raman scattering, photoluminescence, and SIMS indicate that films on inner divertor wall Tiles 1 and 3, and on floor Tile 4 have some differences in the chemical structure of the deposited films. These data show that Tile 3 has a lower coordination of carbon.

## Acknowledgements

This work has been conducted under the European Fusion Development Agreement and is partly funded by EURATOM, the National Technology Agency of Finland and the UK Engineering and Physical Sciences Research Council. L. Khriachtchev thanks support from the Academy of Finland partially through CoE CMS.

## References

[1] J.P. Coad, N. Bekris, J.D. Elder, S.K. Erents, D.E. Hole, K.D. Lawson, G.F. Matthews, R.-D. Penzhorn, P.C. Stangeby, J. Nucl. Mater. 290–293 (2001) 224.
[2] J.P. Coad, P.L. Andrew, et al., in: 26th EPS Conference on Controlled Fusion and Plasma Physics, Maastricht, June 1999.
[3] S.K. Erents, A.V. Chankin, G.F. Matthews, P.C. Stangeby, Plasma Phys. Contr. Fusion 42 (2000) 905.
[4] J. Likonen, S. Lehto, J.P. Coad, T. Renvall, T. Sajavaara, T. Ahlgren, D.E. Hole, G.F. Matthews, J. Keinonen, Fusion Eng. Des. 66–68 (2003) 219.
[5] M. Yoshikawa, Mater. Sci. Forum 52&53 (1989) 365.
[6] M.A. Tamor, W.C. Vassell, J. Appl. Phys. 76 (1994) 3823.
[7] L. Khriachtchev, Top. Appl. Phys. 100 (2006) 403.
[8] J.F. Ziegler, SRIM-96 computer code, private communication.
[9] J.P. Coad, J. Likonen, M. Rubel, E. Vainonen-Ahlgren, D.E. Hole, T. Sajavaara, T. Renvall, G. Matthews, Nucl. Fusion 46 (2006) 350.
[10] J. Likonen, J.P. Coad, E. Vainonen-Ahlgren, T. Renvall, D.E. Hole, M. Rubel, A. Widdowson, J. Nucl. Mater. 363–365 (2007) 190.
[11] M. Mayer, SIMNRA User's Guide, Report IPP 9/113, Max-Planck-Institut für Plasmaphysik, Garching, Germany, 1997.
[12] P. Sander, M. Altebockwinkel, W. Storm, L. Wiedmann, A. Benninghoven, J. Vac. Sci. Technol. B 7 (1989) 517.
[13] A. Benninghoven, F.G. Rüdenauer, H.W. Werner, Secondary Ion Mass Spectrometry, Wiley, New York, 1987.
[14] B.J. Garrison, N. Winograd, D.E. Harrison, J. Chem. Phys. 69 (1978) 1440.
[15] N. Winograd, D.E. Harrison, B.J. Garrison, Surf. Sci. 78 (1978) 467.
[16] L. Khriachtchev, R. Lappalainen, M. Hakovirta, M. Räsänen, Diamond Relat. Mater. 6 (1997) 694.
[17] J. Wagner, P. Lautenschlager, J. Appl. Phys. 59 (1986) 2044.
[18] A.V. Stanishevsky, L.Yu. Khriachtchev, R. Lappalainen, M. Räsänen, Diamond Relat. Mater. 6 (1997) 1026.